Equation of state and force fields for Feynman–Hibbs-corrected Mie fluids. II. Application to mixtures of helium, neon, hydrogen and deuterium

Ailo Aasen,[1,2,a] Morten Hammer,[2] Erich A. Müller,[3] and Øivind Wilhelmsen[1,2]
[1] *Department of Energy and Process Engineering, Norwegian University of Science and Technology, NO-7491 Trondheim, Norway*
[2] *SINTEF Energy Research, NO-7465 Trondheim, Norway*
[3] *Department of Chemical Engineering, Centre for Process Systems Engineering, Imperial College London, South Kensington Campus, London SW7 2AZ, United Kingdom*

(Dated: 12 February 2020)

We extend the SAFT-VRQ Mie equation of state, previously developed for pure fluids [Aasen et al., J. Chem. Phys. **151**, 064508 (2019)], to fluid mixtures of particles interacting via Mie potentials with Feynman–Hibbs quantum corrections of first (Mie-FH1) or second order (Mie-FH2). This is done using a third-order Barker–Henderson expansion of the Helmholtz energy from a non-additive hard-sphere reference system. We survey existing experimental measurements and ab initio calculations of thermodynamic properties of mixtures of neon, helium, deuterium and hydrogen, and use them to optimize the Mie-FH1 and Mie-FH2 force fields for binary interactions. Simulations employing the optimized force fields are shown to follow the experimental results closely over the entire phase envelopes. SAFT-VRQ Mie reproduces results from simulations employing these force fields, with the exception of near-critical states for mixtures containing helium. This breakdown is explained in terms of the extremely low dispersive energy of helium, and the challenges inherent in current implementations of the Barker–Henderson expansion for mixtures. The interaction parameters of two cubic equations of state (SRK, PR) are also fitted to experiments, and used as performance benchmarks. There are large gaps in the ranges and properties that have been experimentally measured for these systems, making the force fields presented especially useful.

I. INTRODUCTION

In Paper I[1] we presented an equation of state for Mie potentials with first- (Mie-FH1) or second-order (Mie-FH2) Feynman–Hibbs quantum corrections, called SAFT-VRQ Mie. It was shown to accurately reproduce the thermodynamic properties of these potentials, denoted collectively as Mie-FH potentials, with a similar accuracy as present state-of-the-art for classical (uncorrected) Mie potentials.[2] We found the optimal Mie-FH1 and Mie-FH2 potential parameters for the pure fluids helium, neon, deuterium, normal-, ortho and para-hydrogen by fitting the Mie-FH1 and Mie-FH2 potentials to thermodynamic data. With no new adjustable parameters, the Mie-FH potentials were shown to be more accurate models for these pure fluids than classical Mie potentials, representing their thermodynamic properties to high accuracy except for pressurized helium below 20 K.

The present paper builds on Paper I and extends the framework to fluid mixtures of helium, neon, hydrogen, as well as their isotopologues and spin isomers. These *ultracryogenic* fluids exhibit stable vapor–liquid equilibria below 50 K, and have been touted as key to increase the efficiency in large-scale hydrogen liquefaction processes.[3,4] One reason is that adding neon to the mixture increases its molecular weight, so that highly efficient turbo compressors can be used instead of piston compressors.[3] Another advantage of using neon mixtures as a refrigerant at low temperatures is the enhanced heat transfer coefficient due to evaporation and condensation;[4] accurate prediction of phase equilibria for these fluids is crucial for this application. Hydrogen–neon and deuterium–neon mixtures are also used in bubble chambers to detect gamma rays.[5,6] Furthermore, when liquid hydrogen is used as fuel for vehicles[7] or space rockets,[8] helium is a preferred choice for pressurization and expulsion since other components will solidify. For this application, the solubility of helium in the liquid hydrogen is needed at low temperatures.

There is little work in the literature on modeling the thermodynamic properties of ultracryogenic fluid mixtures and, to our knowledge, no accurate model currently exists. Wilhelmsen et al.[4] tested several EoS for modeling the phase equilibria of helium–neon mixtures, such as cubic EoS with advanced mixing rules,[9–11] sophisticated corresponding-states EoS such as SPUNG,[12] and PC-SAFT.[13] None of these EoS yielded good agreement with measurements. For pure fluids, however, accurate reference-grade equations of state exist for helium,[14] neon,[15] ortho-, para- and normal-hydrogen,[16] and deuterium.[17] These *multiparameter* EoS are sophisticated correlations of experimental data aiming to fulfill all thermodynamic consistency criteria.[18] However, already for pure fluids these EoS come with challenges[19] that hinder their widespread use. These challenges are amplified for mixtures, and currently one lacks the binary mixing models needed to extend multiparameter EoS to ultracryogenic fluid mixtures. The current paucity of experimental data exacerbates the problem of designing such mixing models.

[a] Electronic mail: ailo.aasen@ntnu.no

Perturbation theory and SAFT-type EoS, on the other hand, are readily extended to mixtures.[2,20] Moreover, a major advantage of EoS based on interaction potentials is that molecular simulations of the underlying force field can be leveraged to estimate transport properties such as viscosity, thermal conductivity, or interfacial properties such as the surface tension or the Kapitza resistance.[21] Furthermore, simulations can be used to obtain thermodynamic properties in regions outside of the domain of validity of the EoS.

Following Barker and Henderson's seminal works on perturbation theory[22,23] for pure substances, Leonard et al.[20] shortly thereafter extended it to mixtures. Since then, the theory has been successfully applied to a variety of fluid mixtures such as electrolyte solutions, polymer mixtures, mixtures of cyclic and ring-forming compounds, and much more.[24–27] However, the present work is the first time the theory is used to describe mixtures of quantum-corrected Mie fluids. The hard-sphere contribution turns out to be especially important for these fluids, since their interaction potentials have shallower attractive tails and harder repulsive cores than classical Mie fluids. As a result, we find that details of the perturbation theory that are commonly neglected[2,13] become important.

Although neon is well-represented by a classical Mie potential,[28] hydrogen, deuterium and helium are not.[1] We will therefore not present mixture results for classical Mie potentials; seeing as they mispredict several single-component properties such as density and saturation vapor pressures (except for neon), they cannot yield a satisfactory mixture model. We will, however, benchmark our approach against a cubic EoS, namely Soave–Redlich–Kwong (SRK).[9] This is because SRK is both simple and fast,[19] and one needs to know whether the gain in accuracy justifies the higher complexity of the SAFT-VRQ Mie EoS and/or simulations of the underlying force fields. For convenience, we present optimized interaction parameters for the two most common cubic EoS: SRK, and the Peng–Robinson[10] (PR) EoS.

In Sec. II we discuss the Feynman–Hibbs-corrected Mie potential, second virial coefficients for mixtures, and the extension of the perturbation theory from Paper I to mixtures. In Sec. III we provide details on the Monte Carlo simulations and the regression of force-field parameters to binary mixture data. In Sec. IV we survey experimental data on binary mixtures of ultracryogenic fluids, and compare them with simulations of the optimized force fields and the predictions of SAFT-VRQ Mie. Concluding remarks are given in Sec. V.

II. THEORY

A. The Feynman–Hibbs-corrected Mie potential

The complete expression for the quantum-corrected Mie-FH2 potential between particles of type i and j is

$$\begin{aligned} u_{ij}(r,\beta)/(\mathcal{C}(\lambda_{\mathrm{r},ij},\lambda_{\mathrm{a},ij})\epsilon_{ij}) &= \frac{(\sigma_{ij})^{\lambda_{\mathrm{r},ij}}}{r^{\lambda_{\mathrm{r},ij}}} - \frac{(\sigma_{ij})^{\lambda_{\mathrm{a},ij}}}{r^{\lambda_{\mathrm{a},ij}}} \\ &+ D_{ij}\left(Q_1(\lambda_{\mathrm{r},ij})\frac{(\sigma_{ij})^{\lambda_{\mathrm{r},ij}}}{r^{\lambda_{\mathrm{r},ij}+2}} - Q_1(\lambda_{\mathrm{a},ij})\frac{(\sigma_{ij})^{\lambda_{\mathrm{a},ij}}}{r^{\lambda_{\mathrm{a},ij}+2}}\right) \\ &+ D_{ij}^2\left(Q_2(\lambda_{\mathrm{r},ij})\frac{(\sigma_{ij})^{\lambda_{\mathrm{r},ij}}}{r^{\lambda_{\mathrm{r},ij}+4}} - Q_2(\lambda_{\mathrm{a},ij})\frac{(\sigma_{ij})^{\lambda_{\mathrm{a},ij}}}{r^{\lambda_{\mathrm{a},ij}+4}}\right), \end{aligned} \tag{1}$$

where $\beta = 1/k_{\mathrm{B}}T$, k_{B} is Boltzmann's constant, T is temperature, and

$$\mathcal{C}(\lambda_{\mathrm{r}},\lambda_{\mathrm{a}}) = \left(\frac{\lambda_{\mathrm{r}}}{\lambda_{\mathrm{r}}-\lambda_{\mathrm{a}}}\right)\left(\frac{\lambda_{\mathrm{r}}}{\lambda_{\mathrm{a}}}\right)^{\frac{\lambda_{\mathrm{a}}}{\lambda_{\mathrm{r}}-\lambda_{\mathrm{a}}}}, \tag{2}$$

$$D_{ij} = \frac{\beta\hbar^2(m_i^{-1}+m_j^{-1})}{24}, \tag{3}$$

$$Q_1(\lambda) = \lambda(\lambda-1), \tag{4}$$

$$Q_2(\lambda) = \frac{1}{2}(\lambda+2)(\lambda+1)\lambda(\lambda-1), \tag{5}$$

where m_i is the mass of component i, and $\hbar = h/2\pi$ is the reduced Planck's constant. The expressions for the Mie-FH1 potential are obtained by omitting the term in Eq. (1) with the prefactor D_{ij}^2, whereas the classical Mie potential is obtained by also omitting the term with prefactor D_{ij}.

We have used the same combining rules that are commonly used for classical Mie fluids:[2]

$$\lambda_{k,ij} - 3 = \sqrt{(\lambda_{k,ii}-3)(\lambda_{k,jj}-3)}, \quad k = \mathrm{a},\mathrm{r}, \tag{6}$$

$$\sigma_{ij} = (1-l_{ij})\frac{\sigma_{ii}+\sigma_{jj}}{2}, \tag{7}$$

$$\epsilon_{ij} = (1-k_{ij})\frac{\sqrt{\sigma_{ii}^3\sigma_{jj}^3}}{\sigma_{ij}^3}\sqrt{\epsilon_{ii}\epsilon_{jj}}, \tag{8}$$

where k_{ij} and l_{ij} are adjustable parameters that will be fitted to experimental data on binary mixtures. The pure-component parameters for helium, neon, deuterium and hydrogen are fixed to be as in Paper I.

For classical Mie potentials, $-\epsilon_{ij}$ is the minimum value of the potential, and σ_{ij} is the distance at which the potential is zero. For the Mie-FH1 and Mie-FH2 potentials, we define the analogous quantities $\epsilon_{ij,\mathrm{eff}}$ and $\sigma_{ij,\mathrm{eff}}$ by the equations

$$u_{ij}(\sigma_{ij,\mathrm{eff}},\beta) = 0, \tag{9}$$

$$\epsilon_{ij,\mathrm{eff}} = -\min_r\left(u_{ij}\left(r,\beta\right)\right), \tag{10}$$

which both vary with temperature. As explained in Paper I, for Mie-FH potentials we have the general relations

This is the accepted version of an article publishet in Journal of Chemical Physics
http://dx.doi.org/10.1063/1.5136079

$\epsilon_{ij,\mathrm{eff}} \leq \epsilon_{ij}$ and $\sigma_{ij,\mathrm{eff}} \geq \sigma_{ij}$, with equality being reached only in the limit $T \to \infty$.

Finally, we define the dimensionless van der Waals energy of the ij interaction as

$$\alpha_{ij} = -\frac{1}{\epsilon_{ij,\mathrm{eff}}\sigma_{ij,\mathrm{eff}}^3} \int_{\sigma_{ij,\mathrm{eff}}}^{\infty} u_{ij}\left(r,\beta\right) r^2 \,\mathrm{d}r\,. \tag{11}$$

B. Extending the perturbation theory from Paper I to mixtures

We shall apply the Barker–Henderson perturbation theory[20,23,29] to obtain an equation of state for multicomponent fluids of particles interacting through the pair potential described in Sec. II A. The reduced, residual Helmholtz energy $a^{\mathrm{res}} = A/Nk_{\mathrm{B}}T$, where N is the number of particles, is given by

$$a^{\mathrm{res}} = a^{\mathrm{HS}} + \beta a_1 + \beta^2 a_2 + \beta^3 a_3, \tag{12}$$

where a^{HS} is the reduced, residual Helmholtz energy of a reference system of hard-spheres to be specified below, while a_1, a_2 and a_3 are the first-, second- and third-order perturbation coefficients.

The procedure for obtaining the four terms in Eq. (12) is well-known for pure fluids,[2,30] and was carried out in Paper I for pure Mie-FH1 and Mie-FH2 fluids. The theory for *mixtures* was first presented by Leonard et al.,[20] who derived the theory for several choices of reference systems. In this work we shall use a reference system that is a mixture of hard spheres where component pair ij interacts with diameter d_{ij}, where

$$d_{ij} = \int_0^{\sigma_{ij,\mathrm{eff}}} \left[1 - \exp\{-\beta u_{ij}(z,\beta)\}\right] \mathrm{d}z\,. \tag{13}$$

The fact that generally $d_{ij} \neq (d_{ii} + d_{jj})/2$ means that the reference is a mixture of *non-additive* hard spheres.

As far as we are aware, the current work is the first implementation of perturbation theory for a non-additive reference system. The main reason for this will become clear in Sec. IV, where we will encounter binary systems for which d_{ij} is significantly different from $(d_{ii} + d_{jj})/2$. Current implementations of perturbation theory using an additive reference system are in these cases inaccurate; although a more accurate implementation of the perturbation theory might improve this, currently the non-additive hard-sphere reference system is superior.

We next detail how to calculate the four terms in Eq. (12).

1. The hard-sphere term

The EoS by Santos et al.[31] is used to model the Helmholtz energy density a^{HS} of the non-additive hard-sphere mixture interacting with diameters d_{ij}. Whereas several other models exist,[32] the model by Santos et al. is highly accurate and was constructed to provide the correct second and third mixture virial coefficients of non-additive hard-sphere mixtures.[31]

The non-additive mixture hard-sphere diameter is given as

$$d_{\mathrm{na}} = \left(\sum_i x_i d_{ii}^3\right)^{1/3}, \tag{14}$$

where x_i is the mole fraction of component i, and the corresponding packing fraction is

$$\eta_{\mathrm{na}} = \frac{\pi\rho d_{\mathrm{na}}^3}{6}, \tag{15}$$

where ρ is the density. The residual compressibillity factor is modeled as

$$\begin{aligned} Z_{\mathrm{na}}^{\mathrm{res}} =& \frac{\eta_{\mathrm{na}}}{1-\eta_{\mathrm{na}}} \frac{10 d_{\mathrm{na}}^3 \overline{B_2} - 4\overline{B_3}}{6 d_{\mathrm{na}}^6} \\ &+ Z_{\mathrm{pure}}^{\mathrm{res}}\left(\eta_{\mathrm{na}}\right) \frac{\overline{B_3} - d_{\mathrm{na}}^3 \overline{B_2}}{6 d_{\mathrm{na}}^6}, \end{aligned} \tag{16}$$

where

$$\overline{B_2} = 4 \sum_i \sum_j x_i x_j d_{ij}^3\,, \tag{17}$$

$$\overline{B_3} = \sum_i \sum_j \sum_k x_i x_j x_k \overline{B}_{ijk}^3\,, \tag{18}$$

and $\overline{B}_{ijk}$ is given by

$$\overline{B}_{ijk} = \frac{4}{3}\left(c_{k;ij} d_{ij}^3 + c_{j;ik} d_{ik}^3 + c_{i;jk} d_{jk}^3\right), \tag{19}$$

$$c_{k;ij} = \delta_{k;ij}^3 + \frac{3}{2}\frac{\delta_{k;ij}^2}{d_{ij}} \delta_{i;jk}\delta_{j;ik}\,, \tag{20}$$

$$\delta_{k;ij} = \max\left(d_{ik} + d_{jk} - d_{ij}, 0\right). \tag{21}$$

Defining the volume-independent quantities

$$A_1\left(T,\boldsymbol{x}\right) = \frac{10 d_{\mathrm{na}}^3 \overline{B_2} - 4\overline{B_3}}{6 d_{\mathrm{na}}^6}, \tag{22}$$

$$A_2\left(T,\boldsymbol{x}\right) = \frac{\overline{B_3} - d_{\mathrm{na}}^3 \overline{B_2}}{6 d_{\mathrm{na}}^6}, \tag{23}$$

the reduced, residual Helmholtz energy becomes

$$\begin{aligned} a^{\mathrm{HS}} &= \int_V^{\infty} \frac{Z_{\mathrm{na}}^{\mathrm{res}}}{V}\,\mathrm{d}V \\ &= -\ln\left(1-\eta_{\mathrm{na}}\right) A_1\left(T,\boldsymbol{x}\right) + a_{\mathrm{pure}}(\eta_{\mathrm{na}}) A_2\left(T,\boldsymbol{x}\right). \end{aligned} \tag{24}$$

We have used the Carnahan–Starling EoS[33] for the reduced residual Helmholtz energy of the pure fluid, a_{pure}.

This is the accepted version of an article publishet in Journal of Chemical Physics
http://dx.doi.org/10.1063/1.5136079

2. The first-order perturbation term

The first-order perturbation term is calculated as

$$a_1 = \sum_i \sum_j x_i x_j a_{1,ij}, \tag{25}$$

where $a_{1,ij}$ is given by

$$a_{1,ij} = 2\pi\rho \int_{\sigma_{ij,\mathrm{eff}}}^{\infty} g_{ij}^{\mathrm{HS,mix}}\left(z;\rho,\boldsymbol{x},\beta\right) u_{ij}\left(z,\beta\right) z^2 \,\mathrm{d}z\,. \tag{26}$$

Here $g_{ij}^{\mathrm{HS,mix}}(z)$ is the radial distribution function of components i and j in the hard-sphere reference mixture at separation z. In addition to depending on density ρ and mole fractions $\boldsymbol{x} = (x_1, x_2, \ldots)$, it also depends on temperature through the hard-sphere diameters (cf. Eq. (13)).

Although Eqs. (25)–(26) are exact, $g_{ij}^{\mathrm{HS,mix}}$ is unknown and must be approximated. There exist several expressions such as Eqs. 27 and 31 in Ref. 31 that can be used, but these would increase the complexity of the model significantly. We will instead employ the simpler approximation of Lafitte et al.,[2] substituting $g_{ij}^{\mathrm{HS,mix}}$ with the radial distribution function of a *single-component* hard-sphere fluid at the temperature of the mixture and an effective packing fraction. More specifically, we set

$$g_{ij}^{\mathrm{HS,mix}}(z;\rho,\boldsymbol{x},\beta) \approx g_{d_{ij}}^{\mathrm{HS,pure}}(z;\eta_{ij}) \tag{27}$$

where $g_{d_{ij}}^{\mathrm{HS,pure}}(z;\eta_{ij})$ is the radial distribution function in a pure system of hard spheres of diameters d_{ij}, at the packing fraction

$$\eta_{ij} = \frac{\pi\rho d_{ij}^3}{6}. \tag{28}$$

We therefore have

$$a_{1,ij} \approx 2\pi\rho \int_{\sigma_{ij,\mathrm{eff}}}^{\infty} g_{d_{ij}}^{\mathrm{HS,pure}}(z;\eta_{ij}) u_{ij}\left(z,\beta\right) z^2 \,\mathrm{d}z\,. \tag{29}$$

To simplify further, note that Eq. (1) is a linear combination of Sutherland potentials, i.e. we can write

$$u_{ij}(r) = \mathcal{C}(\lambda_{\mathrm{r},ij},\lambda_{\mathrm{a},ij}) \sum_k w_{ijk} u_{ij}^{\mathrm{S}}(r;\lambda_{ijk}), \tag{30}$$

where the Sutherland potentials are defined by

$$u_{ij}^{\mathrm{S}}\left(r;\lambda_{ijk}\right) = -\epsilon_{ij}\left(\frac{\sigma_{ij}}{r}\right)^{\lambda_{ijk}}. \tag{31}$$

The prefactors w_{ijk} are given in Tab. I. Since the expression in Eq. (29) for $a_{1,ij}$ is linear in u_{ij}, we can combine it with Eq. (30) to write

$$a_{1,ij} = \mathcal{C}(\lambda_{\mathrm{r},ij},\lambda_{\mathrm{a},ij}) \sum_k w_{ijk} a_{1,ijk} \tag{32}$$

k	λ_{ijk}	w_{ijk}
1	$\lambda_{\mathrm{a},ij}$	1
2	$\lambda_{\mathrm{r},ij}$	-1
3	$\lambda_{\mathrm{a},ij}+2$	$D_{ij}Q_1\left(\lambda_{\mathrm{a},ij}\right)/\sigma_{ij}^2$
4	$\lambda_{\mathrm{r},ij}+2$	$-D_{ij}Q_1\left(\lambda_{\mathrm{r},ij}\right)/\sigma_{ij}^2$
5	$\lambda_{\mathrm{a},ij}+4$	$D_{ij}^2Q_2\left(\lambda_{\mathrm{a},ij}\right)/\sigma_{ij}^4$
6	$\lambda_{\mathrm{r},ij}+4$	$-D_{ij}^2Q_2\left(\lambda_{\mathrm{r},ij}\right)/\sigma_{ij}^4$

TABLE I. λ_{ijk} and w_{ijk} coefficients.

where we now only need expressions for $a_{1,ijk}$. For the Mie-FH1 potential we have $k \in \{1,2,3,4\}$, while for Mie-FH2 we have $k \in \{1,\ldots,6\}$.

It was shown in Paper I and Ref. 2 that, for single-component fluids, each $a_{1,ijk}$ can be correlated using two quantities called a_1^{S} and B. We extend these to mixtures in the same way as Ref. 2, and refer the reader to Ref. 2 and Paper I for details. We have that

$$a_{1,ijk} = (x_{0,ij})^{\lambda_{ijk}}\left[a_{1,ijk}^{\mathrm{S}} + B_{ijk}\right], \tag{33}$$

where

$$a_{1,ijk}^{\mathrm{S}} = -12\eta_{ij}\epsilon_{ij}\left(\frac{1}{\lambda_{ijk}-3}\right)\frac{1-\eta_{\mathrm{eff}}\left(\zeta_x;\lambda_{ijk}\right)/2}{\left(1-\eta_{\mathrm{eff}}\left(\zeta_x;\lambda_{ijk}\right)\right)^3}, \tag{34}$$

$$B_{ijk} = 12\eta_{ij}\epsilon_{ij}\left(\frac{1-\zeta_x/2}{\left(1-\zeta_x\right)^3}I_{ijk} - \frac{9\zeta_x\left(1+\zeta_x\right)}{2\left(1-\zeta_x\right)^3}J_{ijk}\right). \tag{35}$$

The rest of the quantities in Eqs. (34)–(35) are defined as follows: We have

$$x_{0,ij} = \frac{\sigma_{ij,\mathrm{eff}}}{d_{ij}}, \tag{36}$$

and

$$I_{ijk} = -\frac{x_{0,ij}^{(3-\lambda_{ijk})}-1}{\lambda_{ijk}-3}, \tag{37}$$

$$J_{ijk} = -\frac{x_{0,ij}^{(4-\lambda_{ijk})}\left(\lambda-3\right) - x_{0,ij}^{(3-\lambda_{ijk})}\left(\lambda_{ijk}-4\right)-1}{\left(\lambda_{ijk}-3\right)\left(\lambda_{ijk}-4\right)}. \tag{38}$$

The effective packing fraction is given by

$$\eta_{\mathrm{eff}}\left(\zeta_x;\lambda\right) = c_1\left(\lambda\right)\zeta_x + c_2\left(\lambda\right)\zeta_x^2 + c_3\left(\lambda\right)\zeta_x^3 + c_4\left(\lambda\right)\zeta_x^4, \tag{39}$$

where ζ_x is the mixture packing fraction, given by

$$\zeta_x = \sum_i \sum_j x_i x_j \eta_{ij}\,. \tag{40}$$

3. The second-order perturbation term

The second-order perturbation term is calculated as

$$a_2 = \sum_i \sum_j x_i x_j a_{2,ij}, \tag{41}$$

This is the accepted version of an article publishet in Journal of Chemical Physics
http://dx.doi.org/10.1063/1.5136079

where $a_{2,ij}$ is approximated by the following expression (cf. Paper I):

$$a_{2,ij} = \pi\rho K^{\mathrm{HS}} (1+\chi_{ij}) \times \int_{\sigma_{ij,\mathrm{eff}}}^{\infty} g_{d_{ij}}^{\mathrm{HS,pure}}(z;\eta_{ij}) \left(u_{ij}(z,\beta)\right)^2 z^2 \,\mathrm{d}z\,. \quad (42)$$

Since $\left(u_{ij}(z,\beta)\right)^2$ is a sum of Sutherland potentials, the integral can be treated in the same manner as for $a_{1,ij}$, where the Sutherland integrals are described as functions of η, ζ_x and x_0 (see Paper I and Ref. 2 for further details). The same isothermal compressibillity K^{HS} of the pure hard-sphere EoS[33] is used for all pair contributions, obtained by substituting the pure-fluid packing fraction η with the mixture packing fraction ζ_x:

$$K^{\mathrm{HS}} = \frac{(1-\zeta_x)^4}{1+4\zeta_x+4\zeta_x^2-4\zeta_x^3+\zeta_x^4}. \quad (43)$$

For the correction factor χ_{ij}, we introduce an effective packing fraction based on $\sigma_{ij,\mathrm{eff}}$, which is computed as

$$\bar{\zeta}_x = \frac{\pi\rho}{6}\sum_i\sum_j x_i x_j \sigma_{ij,\mathrm{eff}}^3\,, \quad (44)$$

giving the following correlation for χ_{ij},

$$\chi_{ij} = f_1(\alpha_{ij})\,\bar{\zeta}_x + f_2(\alpha_{ij})\left(\bar{\zeta}_x\right)^5 + f_3(\alpha_{ij})\left(\bar{\zeta}_x\right)^8. \quad (45)$$

The definitions of f_1, f_2 and f_3 are given in Ref. 2.

4. The third-order perturbation term

Similar to Ref. 2, the third-order perturbation term is calculated using a van der Waals mixing rule,

$$a_3 = \sum_i\sum_j x_i x_j a_{3,ij}\,, \quad (46)$$

where the pair contribution is given as

$$a_{3,ij} = -\epsilon_{ij,\mathrm{eff}}^3 f_4(\alpha_{ij})\,\bar{\zeta}_x \exp\left(f_5(\alpha_{ij})\,\bar{\zeta}_x + f_6(\alpha_{ij})\,\bar{\zeta}_x^2\right). \quad (47)$$

The definitions of f_4, f_5 and f_6 are given in Ref. 2.

C. Computing second virial coefficients

The virial expansion can be expressed in terms of the pressure:

$$\frac{\beta P(T,\rho,\boldsymbol{x})}{\rho} = 1 + B(T,\boldsymbol{x})\rho + \mathcal{O}(\rho^2), \quad (48)$$

where $\boldsymbol{x}$ is the vector of mole fractions and B is the second mixture virial coefficient. For a mixture, the composition-dependence of the second mixture virial coefficient is known exactly,[34] namely

$$B(T,\boldsymbol{x}) = \sum_i\sum_j x_i x_j B_{ij}(T). \quad (49)$$

For particles interacting with Mie-FH potentials, B_{ij} can be rigorously computed from the expression[34]

$$B_{ij}^{\text{Mie-FH}} = -2\pi\int_0^{\infty}\left[\exp(-\beta u_{ij}(r))-1\right] r^2\,\mathrm{d}r\,. \quad (50)$$

For an equation of state, B_{ij} is given by the derivative

$$B_{ij}^{\mathrm{eos}} = \frac{\beta}{2}\left(\frac{\partial^2 P}{\partial\rho_i\partial\rho_j}\right)_T \quad (51)$$

in the zero-density limit, where $\rho_i = x_i\rho$ is the density of component i. In this work, we shall compare B_{ij}^{eos}, $B_{ij}^{\text{Mie-FH}}$, with the experimental values B_{ij}^{expt}. For the binary systems composed of H_2, D_2 and He, the symbol B_{ij}^{expt} will denote the virial coefficients computed from ab initio calculations. The reason that we treat virial coefficients from ab initio calculations on the same level as experimental measurements is that, for He, H_2, and D_2, the quantum-mechanical calculations can be performed with an accuracy that exceeds what is possible with current experimental techniques.[35,36]

D. Cubic equations of state

The calculations with the SRK[9] and PR[10] equations of state have been performed with the classical alpha correlations, the quadratic mixture rule, and no volume shift. We refer the reader to Refs. 37–39 for details on these models. Note that volume shifts were tested in Paper I for pure neon and hydrogen, and found to not significantly improve the density predictions.

III. METHODS

A. Gibbs Ensemble Monte Carlo simulations

We performed Gibbs Ensemble Monte Carlo (GEMC) simulations[40–42] of binary mixtures of Mie-FH1 and Mie-FH2 fluids to determine two-phase coexistence densities and compositions. This simulation method involves two simulation boxes, one for each phase, that are subjected to three types of Monte Carlo (MC) moves: (i) displacing a particle within a box; (ii) swapping a particle from one box to the other; (iii) isotropically expanding/contracting a box volume. Whereas the GEMC method for pure components preserves the total volume of the simulation boxes, for binary mixtures this is unnecessary,[40] and in this work we maintained the pressure by adjusting each box volume independently.

This is the accepted version of an article publishet in Journal of Chemical Physics
http://dx.doi.org/10.1063/1.5136079

A number $N_{\rm tot}$ of particles in the range 3000–5000 were distributed across the two simulation boxes, with the ratio of each species in the boxes being equal to the phase equilibrium compositions predicted by SAFT-VRQ Mie. The sequence of MC moves was randomized, with the ratio of moves (i):(ii):(iii) initialized to $N_{\rm tot}$:$N_{\rm tot}$:2. The swap move was performed by choosing one of the boxes with equal probability, randomly (but not equiprobably) choosing which species to attempt swapping, and then choosing a random particle of that species and attempting to move it to the other box. During an equilibration stage, the relative probability of which species to attempt swapping was adjusted to yield an equal number of *successful* swaps for each species. The volume moves were performed as random walks in the logarithm of volume.[42] The maximum volume step size was tuned independently for each box to yield an acceptance ratio between 30% and 50%; the maximum displacement step size was tuned independently for each species and each box, to yield an acceptance ratio in the same interval.

We define a Monte Carlo cycle as $N_{\rm tot}$ attempted displacement moves, 2 attempted single-box volume moves, and $N_{\rm swap}$ attempted swap moves. The number $N_{\rm swap}$ was initialized to $N_{\rm tot}$, and increased to ensure that at least 0.1% of the $N_{\rm tot}$ particles were on average exchanged in a cycle. Sampling of densities and compositions was performed after each 100th MC move; although it is conventional to sample only at the end of each cycle, sampling more often is both computationally cheap and increases accuracy. After 3×10^4 equilibration cycles, sampling was performed during 3×10^5 production cycles. The simulations were run with a temperature-independent cutoff of $r_c = 4\sigma$ coupled with on-the-fly long-range corrections as described in the appendix of Paper I, which we extended to mixtures. To gauge the effect of cutoff length, we also ran some of the simulations with the cutoff $r_c = 5\sigma$; the results were equal within the uncertainty.

B. Regression of interaction parameters for real fluids

The adjustable parameters of Mie-FH potentials are the same as for Mie potentials, namely σ, ϵ, $\lambda_{\rm a}$ and $\lambda_{\rm r}$. We have previously presented optimized parameters for pure helium, neon, hydrogen and deuterium for both Mie-FH1 and Mie-FH2 potentials (Tab. II in Paper I). For mixtures, we introduce the two adjustable interaction parameters k_{ij} and l_{ij}, as defined in Eqs. (7)–(8). We also tested the effect of varying the cross-exponent for the repulsive interaction, $\lambda_{{\rm r},ij}$, but concluded that its effect on the predictions can be captured by varying (k_{ij}, l_{ij}).

The interaction parameters were optimized for the accuracy of the force fields, not the accuracy of the equation of state. In addition to yielding more accurate force fields, this approach makes it possible to improve the accuracy of the perturbation theory without having to refit the force-field parameters. Whereas SAFT-VRQ Mie and simulations of the underlying force fields are in excellent agreement away from the critical region, for some mixtures they differ close to a critical point. For this reason, it was infeasible to fit the potential parameters using SAFT-VRQ Mie, as we did not know a priori for which states SAFT-VRQ Mie fails to reproduce the thermodynamic properties of Mie-FH fluids.

We therefore resorted to the more time-consuming job of fitting the force fields directly, i.e. comparing simulation results to experimental data for different values of the interaction parameters. Fortunately, we were able to speed up this process significantly by using measurements[43] and accurate ab initio calculations[35,36] of the cross virial coefficients ($B_{12}^{\rm expt}$) for the binary mixtures. These $B_{12}^{\rm expt}$ values were used to quickly produce a small set of interaction parameters (k_{ij}, l_{ij}) with the property that $B_{12}^{\text{Mie-FH}} \approx B_{12}^{\rm expt}$. Given this small set of (k_{ij}, l_{ij}) values, we chose the optimal value as that which yielded best agreement with phase-composition measurements for the simulations of the force fields.

For real fluids, the intermolecular forces are not exactly pairwise additive, and the optimized Mie-FH potentials we present in this work are *effective* pair potentials – they also implicitly account for three-body and higher-order effects. One might question the use of the second virial coefficient, which is a property only probing two-body interactions,[34] to fit an effective potential that will be influenced by higher-body effects. However, for the fluids and conditions considered in the present work, this is indeed justified: Such effects, if significant, would likely be noticeable already for pure fluids, and we have verified in the Supplementary Material that the optimized parameters of Paper I yield accurate virial coefficients for pure fluids. Moreover, for the binary mixtures considered here, we found that it was possible to obtain good agreement with both the second virial coefficients and the phase equilibrium composition measurements. This indicates that two-body interactions dominate, at least at the moderate pressures considered here, and hence our fitting process is a posteriori justified.

The relevant experimental measurements for these binary systems were all published during the years 1951–1981. In fact, with a few notable exceptions[6,44–46] the 1973 survey of Kidnay et al.[47] is still reasonably up-to-date. To evaluate the quality of the experimental measurements, we checked whether measurements from different publications agree, and whether the mixture data extrapolate to the (accurately known) pure-component data. This extrapolation procedure is facilitated by Henry's law, i.e. that the Pxy phase equilibrium envelope is well-approximated by linear function of finite slope for states close to pure-component saturation states.

IV. RESULTS AND DISCUSSION

The regressed interaction parameters for the six binary combinations of He, Ne, H_2 and D_2 are given in Tab. II,

This is the accepted version of an article publishet in Journal of Chemical Physics
http://dx.doi.org/10.1063/1.5136079

TABLE II. Optimal interaction parameters (k_{ij}, l_{ij}) for the Mie-FH1 potentials for pairs of real fluids.

	D_2	H_2	He
H_2	$(0, 0)$	–	–
He	$(0.0, -0.05)$	$(0.08, -0.05)$	–
Ne	$(0.13, 0)$	$(0.105, 0)$	$(-0.22, 0)$

TABLE III. Optimal interaction parameters (k_{ij}, l_{ij}) for the Mie-FH2 potentials for pairs of real fluids.

	D_2	H_2	He
H_2	$(-0.04, 0)$	–	–
He	$(0.12, -0.05)$	$(0.15, -0.025)$	–
Ne	$(0.14, 0)$	$(0.105, 0)$	$(-0.06, 0)$

Tab. III and Tab. IV. It was only for He–H_2 and He–D_2 that we found it necessary to tune the l_{ij} parameter to accurately reproduce the experimental data.

As mentioned in Paper I, three types of hydrogen are commonly considered:[1,16] orthohydrogen (the two protons have equal spin), parahydrogen (opposite spin), and normal hydrogen which is a 3–1 mixture of ortho- and parahydrogen that represents the equilibrium composition at high temperature. In Paper I, we fitted the intermolecular potential for these three pure fluids, and found that they were very similar. In the present work we will only fit the interaction potential for normal hydrogen with other fluids; if one wants to explicitly model orthohydrogen or parahydrogen as separate components in a mixture, we recommend using the same interaction parameter with other fluids as for normal hydrogen. The interaction parameters between orthohydrogen and parahydrogen, however, should be taken as zero. Three analogous types of deuterium also exist,[17] but here we only treat normal deuterium, i.e. the equilibrium configuration at room temperature.

We now discuss the six binary mixtures separately. In addition, we refer the interested reader to the Supplementary Material for an overview of the global fluid phase behavior in temperature–pressure space, as predicted by SAFT-VRQ Mie with the optimal Mie-FH1 parameters; these show the loci of pure-component saturation, vapor–liquid–liquid equilibria (VLLE), azeotropes and critical points. The calculation and classification of global phase diagrams builds on Refs. 48–50.

TABLE IV. Optimal interaction parameters k_{ij} for the SRK and PR EoS for pairs of real fluids.

	SRK			**PR**		
	D_2	H_2	He	D_2	H_2	He
H_2	0	–	–	0	–	–
He	0.37	0.37	–	0.38	0.37	–
Ne	0.18	0.19	0.10	0.17	0.18	0.15

A. The helium–neon mixture

Two publications report measurements on the helium–neon system: Knorn (1967),[51] and Heck and Barrick (1967),[52] who both measured only phase equilibrium compositions. Unfortunately, the bubble point (i.e. saturated-liquid) measurements from these publications are inconsistent with each other. An example is the bubble point compositions at 26.95 K and 27.03 K, reported by Ref. 52 and Ref. 51 respectively; although the measurements are at essentially the same temperature, they exhibit large and systematic deviations. Moreover, none of the isothermal measurement series can be linearly extrapolated to the pure-component vapor pressures and thus violate Henry's law. That the measurements were taken in the Henry's-law regime is indicated by the fact that the first four bubble point measurements lie on a straight line in Px-space with correlation coefficients above 0.99. Moreover, SAFT-VRQ Mie also predicts an essentially linear bubble point curve in these regions.

The helium–neon mixture is a challenging test of the perturbation theory underlying SAFT-VRQ Mie. Away from the critical point, Figs. 1a–1d show good agreement between GEMC simulations of Mie-FH potentials, predictions by SAFT-VRQ Mie, and experimental measurements. The same good agreement is seen for virial coefficients (Fig. 2). SAFT-VRQ Mie, however, provides inaccurate predictions in the critical region, in some cases overpredicting the critical pressure of Mie-FH fluids by more than 50%. In Ref. 53, we show that, even for simple mixtures of Lennard-Jones fluids, the representations of a_2 and a_3 become inaccurate as the ratio of $\epsilon_{22,\text{eff}}/\epsilon_{11,\text{eff}}$ becomes large. For the Mie-FH1 and the Mie-FH2 potentials this ratio is 7.55 ± 0.1 and 4.3 ± 0.2, respectively, for the temperatures considered in Fig. 1. This explains the overpredictions in the critical region. Improving the representation of a_2 and a_3 is beyond the scope of this work. A different but related aspect of the perturbation theory is the choice of reference system. We found that using a non-additive hard-sphere reference in SAFT-VRQ Mie significantly increased agreement with simulations results for the bubble points in Figs. 1a–1d, compared to using the additive reference by Lafitte et al.[2] The agreement between simulations and SAFT-VRQ Mie is better for the Mie-FH2 potential than for the Mie-FH1 potential, which is especially clear for the phase-equilibrium densities (cf. Figs. 1b and 1d), which might be due to the smaller value of k_{ij}. We refer to Ref. 53 for a further discussion of choice of reference systems.

GEMC simulations of the Mie-FH potentials exhibit better agreement with experimental data than SAFT-VRQ Mie, as they do not suffer from the inadequacies of the EoS in the critical region discussed above. As shown in Fig. 1a and Fig. 1c, simulations of the optimized Mie-FH1 and Mie-FH2 potentials largely agree with the experimental vapor–liquid equilibrium (VLE) composition measurements, including the critical region. The excep-

This is the accepted version of an article publishet in Journal of Chemical Physics
http://dx.doi.org/10.1063/1.5136079

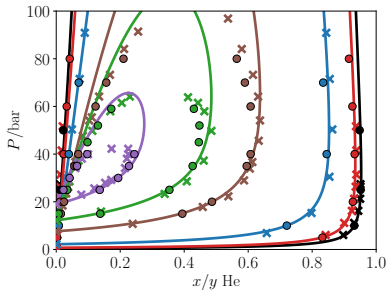

(a) Mie-FH1 Pxy phase diagram.

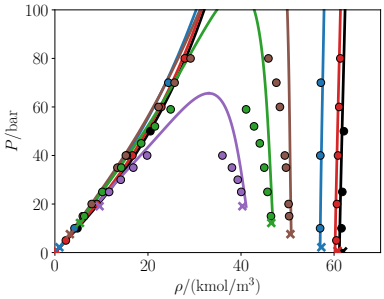

(b) Mie-FH1 $P\rho$ phase diagram.

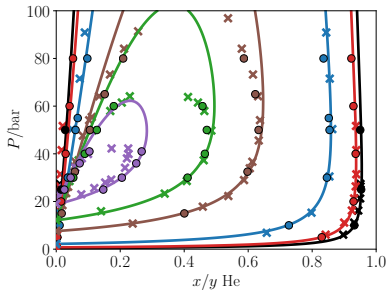

(c) Mie-FH2 Pxy phase diagram.

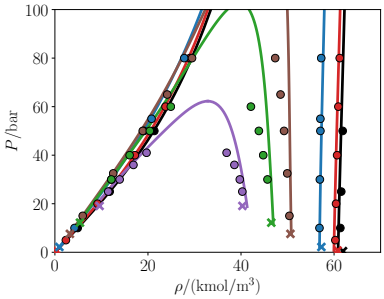

(d) Mie-FH2 $P\rho$ phase diagram.

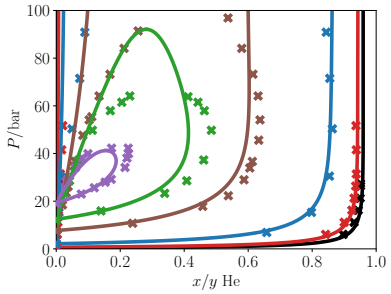

(e) SRK Pxy phase diagram.

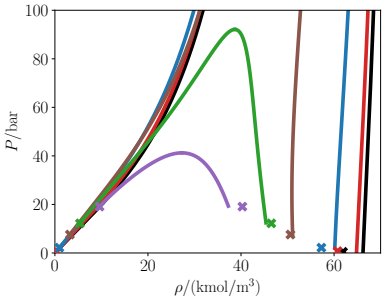

(f) SRK $P\rho$ phase diagram.

FIG. 1. Phase-equilibrium diagrams for the helium–neon mixture using Mie-FH1 potentials (Figs. 1a and 1b), Mie-FH2 potentials (Figs. 1c and 1d) and SRK (Figs. 1e and 1f). Crosses are experimental measurements,[51,52] circles are simulation results, and lines are calculations with SAFT-VRQ Mie (Figs. 1a–1d) or SRK (Figs. 1e–1f). The crosses in the density plots are the pure-component values computed from reference EoS.[14,15] The temperatures are 24.71 K (black), 26.00 K (red), 29.91 K (blue), 35.90 K (brown), 38.80 K (green) and 41.90 K (purple).

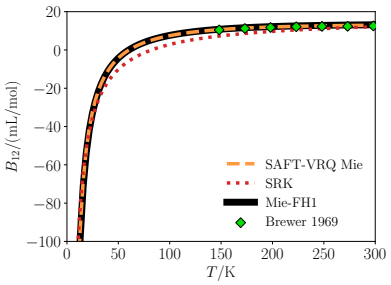

(a) Mie-FH1.

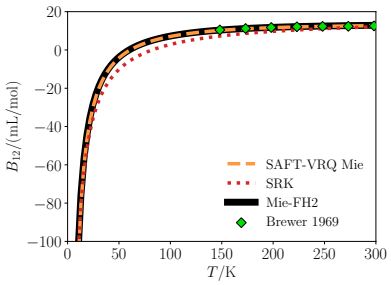

(b) Mie-FH2.

FIG. 2. Cross second virial coefficients for the helium–neon mixture using the Mie-FH1 potential (Fig. 2a) and Mie-FH2 potential (Fig. 2b), compared to predictions by SAFT-VRQ Mie, SRK and measurements by Brewer and Vaughn.[43]

This is the accepted version of an article publishet in Journal of Chemical Physics
http://dx.doi.org/10.1063/1.5136079

tion is states close to the saturation locus of pure neon. However, as explained, these measurements cannot be trusted as they do not extrapolate to the saturation locus of pure neon. Simulations of the Mie-FH potentials (Figs. 1b and 1d) are in our opinion more trustworthy than measurements in this region, especially since they accurately reproduce the saturation locus of pure neon, as shown in Paper I. For this binary mixture, the simulations and SAFT-VRQ Mie agree well with experimental data at temperatures below 30 K. This indicates that the discrepancies at higher temperatures are not due to incorrect modeling of quantum effects, which are stronger at lower temperatures.

SRK fails to accurately reproduce the phase-equilibrium measurements of helium–neon (Figs. 1e–1f), even for pressures below 40 bar. This is in line with the conclusions of Wilhelmsen et al.,[4] who demonstrated that the PR cubic EoS is also unable to accurately model phase-composition measurements. More specifically, they found that a cubic EoS is able to match the phase-composition measurements of either the vapor or the liquid phase, but not both at once; sophisticated interaction rules[11] did not improve on this situation. Fig. 1f illustrates SRK's poor predictions of pure-component liquid densities, which are overestimated at low temperatures and underestimated at high temperatures, and gives a sense of the error that must be expected in density predictions for mixtures. This is in clear contrast to SAFT-VRQ Mie (Figs. 1b and 1d), which is able to accurately predict both saturation vapor pressures and densities for pure components (see Paper I). Finally, Fig. 2 shows that SRK also severely underpredicts the cross second virial coefficient.

B. The hydrogen–neon mixture

The phase behavior of hydrogen–neon is rather exotic: azeotropic VLE at low temperatures, liquid–liquid equilibrium (LLE) at low temperatures and high pressures. The VLE and LLE regimes are separated by three-phase, vapor–liquid–liquid equilibrium (VLLE) states. The interested reader is referred to the Supplementary Material for an overview of the phase behavior in temperature–pressure space. We used the experimental measurements by Streett and Jones (1965)[54] and Heck and Barrick (1966).[55] Streett and Jones found the upper critical solution temperature for the LLE to be 28.96 ± 0.04 K, and measured azeotropes for temperatures up to 31.5 K. We also mention that Simon (1963)[56] reported measurements on parahydrogen–neon system at the triple-point temperature of neon (24.56 K); these data have not been used.

In spite of the complexity of the phase diagram, both simulations and theory are able to describe the mixture, as seen in Figs. 3 and 4. The simulations of the Mie-FH potentials consistently yield a slightly higher mole fraction of hydrogen in both phases than the theoretical predictions by SAFT-VRQ Mie, as well as slightly lower densities of the saturated liquid phase. Overall, however, the correspondence between theory and simulations is good.

SRK seems to be slightly more accurate at reproducing phase composition measurements than the Mie-FH potentials, but less accurate at representing cross virial coefficients. Fig. 3f shows that SRK overestimates liquid densities at low temperatures and underestimates them at high temperatures. SAFT-VRQ Mie and the underlying force fields are clearly more accurate for the densities (Figs. 3b and 3d) than SRK. Fig. 5 compares the measurements of mixture densities and sound speeds by Güsewell et al.[6] to the predictions of SAFT-VRQ Mie and SRK; the Mie-FH1 and Mie-FH2 parameters yield good predictions for both properties, whereas SRK shows higher deviations as well as a wrong variation with temperature.

C. The helium–hydrogen mixture

There is a wealth of measurements on the phase-equilibrium compositions of the helium–hydrogen mixture, even extending up to supercritical fluid–fluid equilibrium at 100 K and 10 000 bars.[44] Curiously, we did not find any measurements on densities of these mixtures, other than those for pure components. In this work we used experimental VLE data by Streett et al. (1964),[57] Sonntag et al. (1964),[58] Sneed et al. (1968),[59] and Streett et al. (1973).[44] All these authors assume that their hydrogen is normal hydrogen, due to the short cooling and sampling times.

The results are plotted in Fig. 6. With $k_{ij} = 0.37$, SRK generally estimates all phase compositions well, although the helium mole fraction in the liquid phase is systematically overpredicted. SRK also mispredicts the pure-component densities, which in turn ruins the mixture density predictions. Simulations of the Mie-FH potentials yield decent agreement with the measurements, with the Mie-FH1 potential being the most accurate. Simulations at 31.50 K (brown curve) of both Mie-FH potentials yield a slightly too high critical pressure compared to measurements.

Whereas SAFT-VRQ Mie is in excellent agreement with simulations away from the critical region, SAFT-VRQ Mie strongly overpredicts the critical pressure for the helium–hydrogen mixture. Once again we attribute this to a deficiency in the description of the critical region as there is, in this case, a large relative difference in the effective potential well-depths. For example, for the temperatures considered in Fig. 6, the ratio $\epsilon_{22,\mathrm{eff}}/\epsilon_{11,\mathrm{eff}}$ equals 4.64 ± 0.02 for Mie-FH1 and 4.15 ± 0.01 for Mie-FH2. Although the critical pressure is overpredicted, also for this system we found that the non-additive hard-sphere reference for SAFT-VRQ Mie improved agreement with simulation results for the saturated liquid.

Since both helium and hydrogen only have two elec-

This is the accepted version of an article publishet in Journal of Chemical Physics
http://dx.doi.org/10.1063/1.5136079

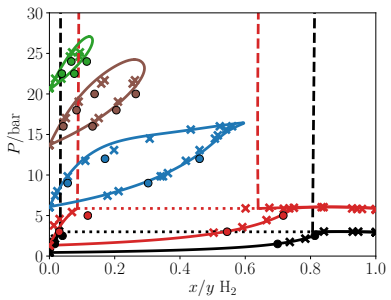

(a) Mie-FH1 Pxy phase diagram.

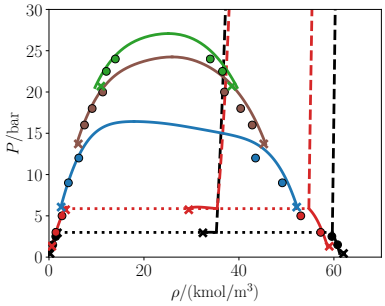

(b) Mie-FH1 $P\rho$ phase diagram.

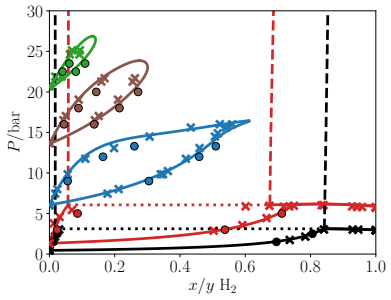

(c) Mie-FH2 Pxy phase diagram.

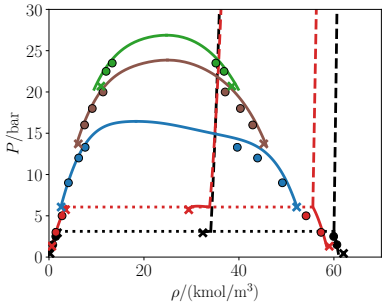

(d) Mie-FH2 $P\rho$ phase diagram.

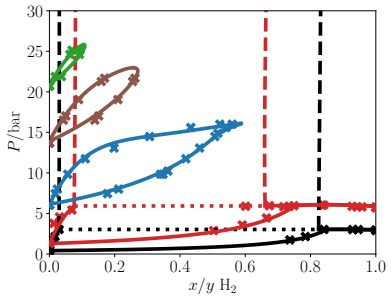

(e) SRK Pxy phase diagram.

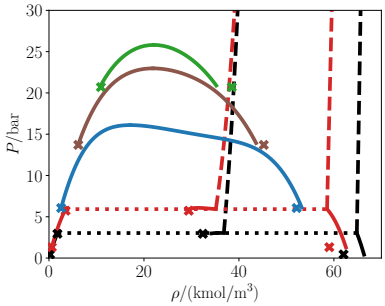

(f) SRK $P\rho$ phase diagram.

FIG. 3. Phase-equilibrium diagrams for the hydrogen–neon mixture using the Mie-FH1 potential (Figs. 3a and 3b) and Mie-FH2 potential (Figs. 3c and 3d). Crosses are experimental measurements,[54,55] circles are simulation results, and lines are calculations with SAFT-VRQ Mie (Figs. 3a–3d) or SRK (Figs. 3e–3f). The full lines are VLE, the dashed lines are LLE, and the dotted lines indicate VLLE. The crosses in the density plots are the pure-component values computed from reference EoS.[15,16] The temperatures are 24.59 K (black), 28.00 K (red), 34.66 K (blue), 39.57 K (brown) and 42.50 K (green).

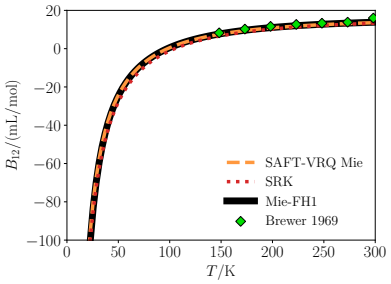

(a) Mie-FH1.

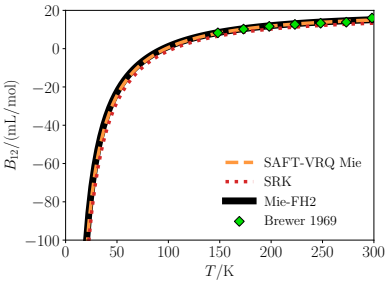

(b) Mie-FH2.

FIG. 4. Cross second virial coefficients for the hydrogen–neon mixture using the Mie-FH1 potential (Fig. 4a) and Mie-FH2 potential (Fig. 4b), compared to predictions of SAFT-VRQ Mie, SRK and measurements by Brewer and Vaughn.[43]

This is the accepted version of an article publishet in Journal of Chemical Physics
http://dx.doi.org/10.1063/1.5136079

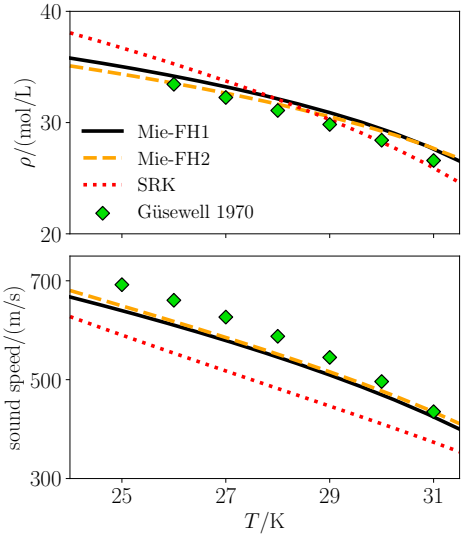

FIG. 5. Liquid densities (top plot) and sound speeds (bottom plot) for the hydrogen–neon mixture at hydrogen mole fraction 0.8. The curves are equation-of-state predictions, from both SRK and SAFT-VRQ Mie using the Mie-FH1 and Mie-FH2 potentials, and the markers are measurements by Güsewell et al.[6]

trons, direct quantum-mechanical ab initio calculations can predict the second virial coefficients B_{12} with an accuracy exceeding what is currently achievable in experiments.[36] Such calculations, which are based on path-integral Monte Carlo simulations,[41] were performed by Garberoglio et al. (2014).[36] Their resulting cross virial coefficients are shown in Fig. 7 as green diamonds, where the uncertainties are smaller than the symbol size. Fig. 7 shows that, for the cross second virial coefficient, the Mie-FH1 potential constitutes an accurate model, while Mie-FH2 and SRK show some deviations. Whereas for Mie-FH1 there is complete agreement between $B_{12}^{\text{Mie-FH}}$ and calculations of B_{12}^{EoS} from SAFT-VRQ Mie, for Mie-FH2 there is a slight mismatch. This mismatch may stem from the second virial coefficient of the Mie-FH2 potential for pure hydrogen being less accurate than that of the Mie-FH1 potential (see the Supplementary Material). We found that when $l_{ij} = 0$, the cross second virial coefficient for the Mie-FH1 potential shows large deviations from the ab initio calculations for *all* values of k_{ij}, and so having $l_{ij} \neq 0$ is in this case essential.

The helium–hydrogen mixture can exhibit barotropic inversion. This means that in certain parts of the VLE region, the liquid phase has lower mass density than the vapor and therefore floats on top of the vapor. Conventional process equipment is not designed for this phenomenon, making it important to predict the conditions where it happens. Fig. 8 shows a comparison of the predicted and measured[59] barotropic inversion curve for the helium–hydrogen mixture. The predictions by SAFT-VRQ Mie lie closer to the measurements than those of SRK, with predictions using the Mie-FH2 potential being the most accurate. The reason that Mie-FH2 is the most accurate model may be its superior accuracy for modeling the density of supercritical helium (cf. Paper I).

D. The helium–deuterium mixture

There are fewer reported measurements on the helium–deuterium mixture than the helium–hydrogen mixture. However, Hiza (1981)[45] has measured the phase equilibrium compositions at pressures up to 20 bar, and the cross second virial coefficients are known to a high accuracy from the ab initio calculations by Garberoglio et al.[36]

SAFT-VRQ Mie overpredicts the saturated liquid helium compositions compared to simulations of the Mie-FH potentials, especially at the lowest temperatures (Figs. 9a and 9c). For example, at 20 K and 20 bar, the Mie-FH1 simulation predicts a helium content $(0.77 \pm 0.1)\%$, whereas SAFT-VRQ Mie predicts 1.15%, and measurements extrapolate to 0.43%. The use of a non-additive hard-sphere reference system in the perturbation theory improves on the additive reference of Lafitte et al.,[2] which underpredicts the helium content for the simulation at 20 K in Fig. 9a by a factor 5 (not shown). Moreover, the low dispersive energy of helium again results in large ratios of $\epsilon_{22,\text{eff}}/\epsilon_{11,\text{eff}}$; for the temperatures plotted in Fig. 9, they are in the range 5.64 ± 0.01 and 3.71 ± 0.5 for the Mie-FH1 and the Mie-FH2 potential, respectively. SAFT-VRQ Mie, in its current implementation, will therefore overpredict the critical pressure.

Overall, simulations of the Mie-FH1 potentials yield best agreement with experimental measurements. All models accurately predict the measured vapor-phase compositions, whereas SRK seems to yield the overall most accurate predictions of liquid-phase compositions. However, SRK overpredicts the liquid densities at the lowest temperature by $\sim$ 20%, whereas the Mie-FH1 model yields highly accurate density predictions. The Mie-FH2 predicts liquid phase compositions with the lowest accuracy of the three models, but is intermediate between Mie-FH1 and SRK for accuracy of density predictions. Whereas both Mie-FH potentials reproduce the cross second virial coefficient well, SRK underpredicts it (Fig. 10).

E. The deuterium–neon mixture

The qualitative phase behavior of the deuterium–neon mixture is similar to that of the hydrogen–neon mixture: azeotropic VLE at low temperatures and LLE at low temperatures and high pressures (Fig. 12). In 1962, Simon published deuterium–neon VLE measurements at the single temperature 24.56 K,[60] i.e. the triple point of neon. Although he also measured second virial coeffi-

This is the accepted version of an article publishet in Journal of Chemical Physics
http://dx.doi.org/10.1063/1.5136079

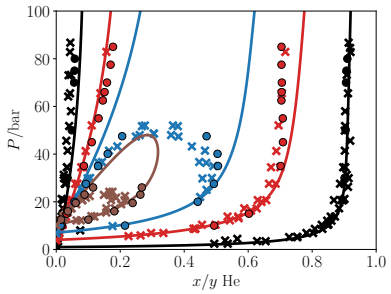

(a) Mie-FH1 Pxy phase diagram.

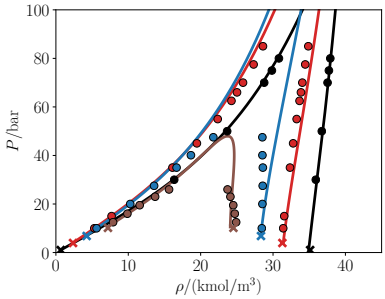

(b) Mie-FH1 $P\rho$ phase diagram.

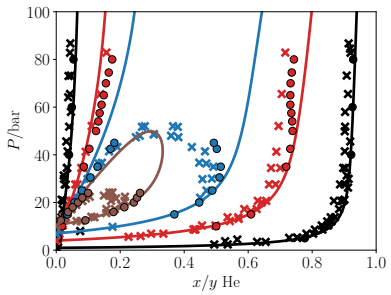

(c) Mie-FH2 Pxy phase diagram.

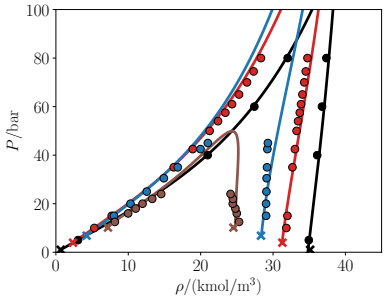

(d) Mie-FH2 $P\rho$ phase diagram.

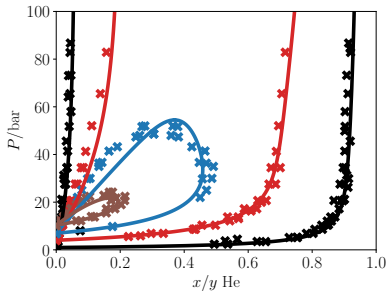

(e) SRK Pxy phase diagram.

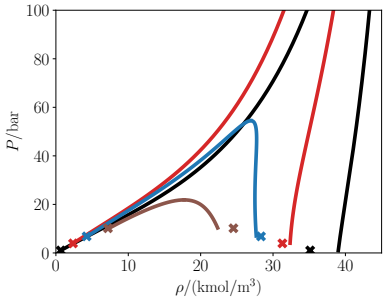

(f) SRK $P\rho$ phase diagram.

FIG. 6. Phase-equilibrium diagrams for the helium–hydrogen mixture using the Mie-FH1 potential (Figs. 6a, 6b) and Mie-FH2 potential (Figs. 6c, 6d). Crosses are experimental measurements,[44,57–59] circles are simulation results, and lines are calculations with SAFT-VRQ Mie (Figs. 6a–6d) or SRK (Figs. 6e–6f). The crosses in the density plots are the pure-component values computed from reference EoS.[14,16] The temperatures are 20.40 K (black), 26.00 K (red), 29.00 K (blue) and 31.50 K (brown).

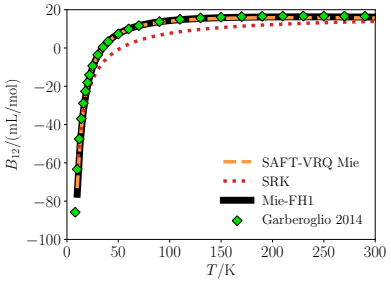

(a) Mie-FH1.

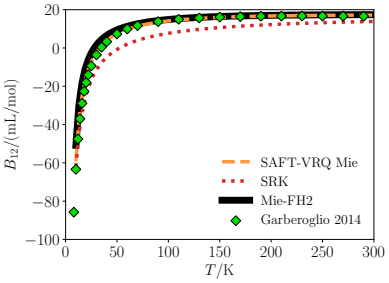

(b) Mie-FH2.

FIG. 7. Cross second virial coefficients for the helium–hydrogen mixture using the Mie-FH1 potential (Fig. 7a) and Mie-FH2 potential (Fig. 7b), compared to predictions of SAFT-VRQ Mie, SRK and ab initio calculations by Garberoglio et al.[36]

This is the accepted version of an article publishet in Journal of Chemical Physics
http://dx.doi.org/10.1063/1.5136079

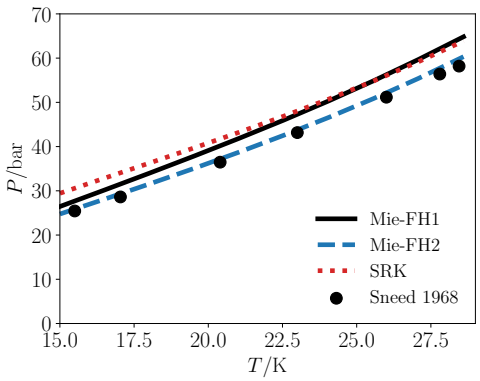

FIG. 8. Barotropic inversion locus for the helium–hydrogen mixture, i.e. the states at which the mass densities of the vapor and liquid phases are equal. Predictions by SRK and SAFT-VRQ Mie with Mie-FH1 and Mie-FH2 potentials, as well as measurements by Sneed et al.[59]

cients, and stated that "more extensive measurements" were in progress, it seems that these measurements were never published. More extensive Pxy measurements were conducted by Streett in 1968.[61] Streett found that the LLE vanishes above the upper critical solution temperature of 25.74 ± 0.03 K,[61] and that azeotropes exist for temperatures up to at least 36.88 K. Streett also conjectured that azeotropes persist all the way up to the vapor–liquid critical locus. Interestingly, SAFT-VRQ Mie using the Mie-FH1 potential makes the same prediction (see Supplementary Material).

The measurements by Simon, and two isotherms by Streett, are shown in Fig. 12 together with predictions by SAFT-VRQ Mie and SRK. Moreover, densities and sound speeds for liquids with deuterium mole fraction are shown in Fig. 11. The takeaway is that the Mie-FH1 and Mie-FH2 models are in excellent agreement with the experimental data, whereas SRK exhibits larger deviations for densities and sound speeds. The deuterium–neon mixture is the only mixture for which we have not found any measurements or ab initio calculations of the cross second virial coefficients. However, Fig. 13 shows that for B_{12}, all models yield very similar predictions, and given the good fit for phase-equilibrium measurements we expect that the predicted second virial coefficients are accurate.

F. The hydrogen–deuterium mixture

Phase-equilibrium composition measurements of the hydrogen–deuterium system were performed by Hoge and Arnold in 1951[62] and by Newman and Jackson[63] in 1958. Studies of this system were initiated to assess the feasibility of separating these two isotopologues by fractional distillation.[64] Since the 1950s, this system has not been studied by experimentalists, but accurate ab initio calculations of virial coefficients were performed by Garberoglio and Harvey[35] in 2013.

Due to the similarity of the two components, the hydrogen–deuterium interaction can be predicted well by simply letting $k_{ij} = l_{ij} = 0.0$ without any fitting. Fig. 14 shows the results for phase-equilibrium calculations. With no fitting parameters, SAFT-VRQ Mie with the Mie-FH1 potential yields excellent predictions for both compositions and densities, and also agrees well with simulations. For the Mie-FH2 potential, a small k_{ij} of -0.04 yields a slightly better match between SAFT-VRQ Mie and the experiments at 23 K and 24 K, and is therefore chosen as the optimal parameter. However, Fig. 14c shows a mismatch between theory and simulations of the Mie-FH2 potential for phase compositions at 28 K. Also, unlike experiments, simulations of the Mie-FH2 potential at 20 K indicate solid formation; this mixture should therefore not be modeled by the Mie-FH2 potentials at such low temperatures. Figs. Figs. 14e–14f show that SRK is able to predict compositions, but overpredicts densities.

Fig. 15 shows that also for this mixture there is an almost exact match between the ab initio calculations and those of the Mie-FH1 potential, Mie-FH2 results being only slightly worse. For both Mie-FH1 and Mie-FH2 there is good agreement with SAFT-VRQ Mie. SRK also yields good predictions of the cross virial coefficient, but is slightly less accurate than SAFT-VRQ Mie.

G. Summary of current challenges of modeling mixtures of ultracryogenic fluids

Before settling on the non-additive hard-sphere reference, we also explored the use of a single-component hard-sphere reference, an additive hard-sphere reference mixture, and the approach by Lafitte et al.[2] We chose the non-additive reference for two reasons: (1) SAFT did not generally reproduce the cross virial coefficients $B_{12}^{\text{Mie-FH}}$ of the underlying force fields without using a *non-additive* hard-sphere reference mixture; (2) compared to the other reference fluids, the non-additive reference resulted in significantly more accurate predictions for high-density liquid states of mixtures containing helium (away from the critical region). The problems of the perturbation theory for mixtures encountered in the present work are not linked to the quantum corrections of the potential, but occur even for binary mixtures of Lennard-Jones fluids.[53] We refer the reader to Ref. 53 for a detailed discussion of these issues, such as the merits of different choices of hard-sphere reference systems, and how to improve accuracy in the critical region.

Independently of how the hard-sphere reference term is modeled, the perturbation theory underlying SAFT-VRQ Mie severely overestimates critical pressures for the binary mixtures involving helium. He atoms have the weakest dispersive attractions of all known substances, reflected in its extremely low critical temperature of 5.2 K. This translates into He having a small value of the

This is the accepted version of an article publishet in Journal of Chemical Physics
http://dx.doi.org/10.1063/1.5136079

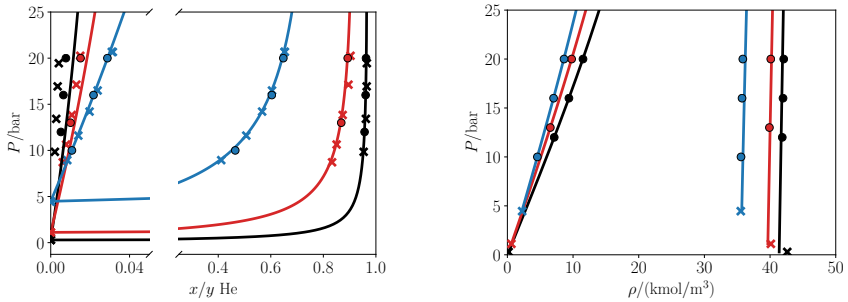

(a) Mie-FH1 Pxy phase diagram.

(b) Mie-FH1 $P\rho$ phase diagram.

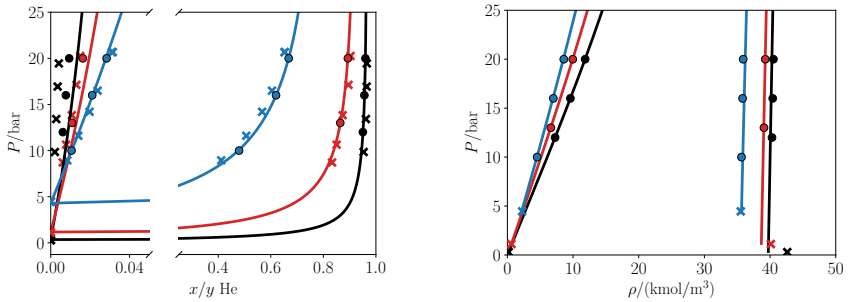

(c) Mie-FH2 Pxy phase diagram.

(d) Mie-FH2 $P\rho$ phase diagram.

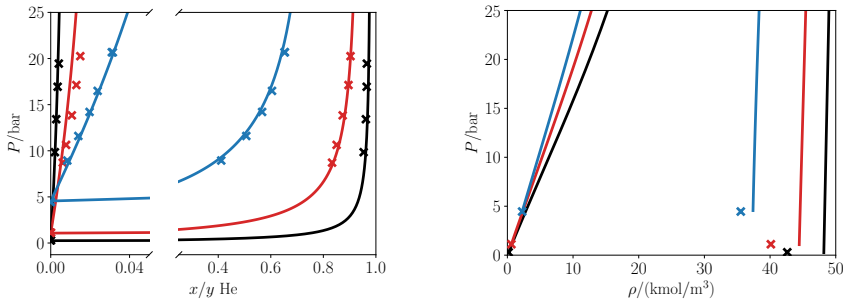

(e) SRK Pxy phase diagram.

(f) SRK $P\rho$ phase diagram.

FIG. 9. Phase equilibrium diagrams for the helium–deuterium mixture using the Mie-FH1 potential (Figs. 9a, 9b) and Mie-FH2 potential (Figs. 9c, 9d). Crosses are experimental measurements,[45] circles are simulation results, and lines are calculations with SAFT-VRQ Mie (Figs. 9a–9d) or SRK (Figs. 9e–9f). Composition plots have been split to magnify the bubble point region. The crosses in the density plots are the pure-component values computed from reference EoS.[14,17] The temperatures are 20 K (black), 24 K (red), and 30 K (blue).

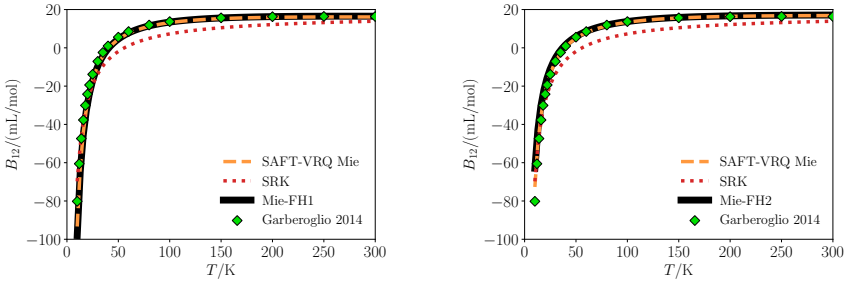

(a) Mie-FH1.

(b) Mie-FH2.

FIG. 10. Cross second virial coefficients for the helium–deuterium mixture using the Mie-FH1 potential (Fig. 10a) and Mie-FH2 potential (Fig. 10b), compared to predictions of SAFT-VRQ Mie, SRK and ab initio calculations by Garberoglio et al.[36]

This is the accepted version of an article publishet in Journal of Chemical Physics
http://dx.doi.org/10.1063/1.5136079

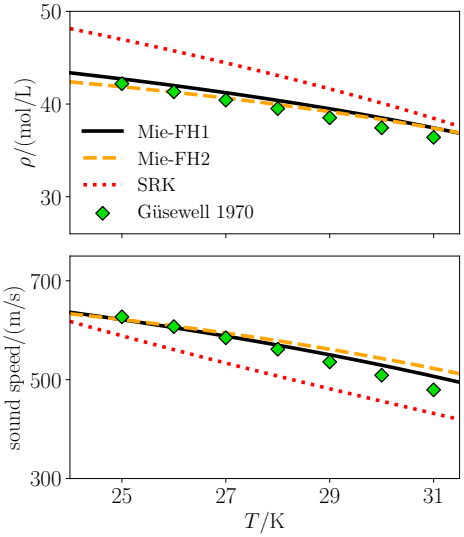

FIG. 11. Liquid densities (top plot) and sound speeds (bottom plot) for the deuterium–neon mixture at deuterium mole fraction 0.7. The curves are equation-of-state predictions, from both SRK and SAFT-VRQ Mie using the Mie-FH1 and Mie-FH2 potentials, and the markers are measurements by Güsewell et al.[6]

(effective) potential well-depth ϵ, resulting in large relative differences in potential well depths for binary mixtures, that the present state-of-the-art representations of the perturbation coefficients a_2 and a_3 cannot handle. For binary mixtures not involving helium, the ratios of the well-depths stay between 0.5 and 2, and the correspondence between simulations and perturbation theory is good. Once again, we stress that these observations also hold for binary mixtures of (classical) Lennard-Jones fluids.[53]

We showed that SRK, using a single binary interaction parameter, can reproduce the phase-composition measurements for all the binary mixtures except helium–neon. The same is true for PR (not shown). This reduces our confidence in the measurements for the helium–neon system further, in addition to their violation of Henry's law discussed in Sec. IV A. In light of their simplicity, the ability of SRK and PR to reproduce experimental Pxy measurements with a single fitting parameter is remarkable. However, as is well documented,[38,65] this accuracy does not hold for other properties such as densities or caloric properties (e.g., heat capacities), although the densities can in some cases be amended using volume shifts.[37] Moreover, the present work shows that SRK consistently underpredicts the second virial coefficient. As shown in Paper I, one of the strengths of the Feynman–Hibbs-corrected Mie fluids and SAFT-VRQ Mie is their capability of accurately reproducing these properties for ultracryogenic fluids. Another strength of Mie-FH potentials is that they allow for studying these fluids from the molecular perspective, which is not possible with a semi-empirical EoS such as SRK.

V. CONCLUSION

The SAFT-VRQ Mie equation of state was successfully extended to mixtures of Mie fluids with Feynman–Hibbs quantum corrections of first and second order. The underlying force fields were fitted to cross second virial coefficients and phase composition measurements of binary mixtures of the ultacryogenic fluids helium, neon, hydrogen and deuterium. These optimized force fields generally exhibit close agreement with experimental data on second virial coefficients and phase equilibrium compositions, as well as densities and sound speeds for the mixtures where measurements of these properties exist. SAFT-VRQ Mie satisfactorily reproduces phase-equilibrium simulations for mixtures not containing helium; for helium mixtures the agreement is satisfactory only at low pressures, whereas critical pressures are severely overestimated. This is a consequence of the representation of the second and third perturbation coefficient in the Barker–Henderson theory, which are inaccurate for the large relative differences in potential well-depths that result from helium's small dispersive energy.

The current implementation of SAFT-VRQ Mie thus has potential for improvement. However, in this work and in Paper I, force-field parameters were optimized for agreement between *simulations* and experimental data. This means that if a more accurate perturbation theory is developed in the future, the force-field parameters can be used without any re-fitting.

Cubic equations of state such as SRK are able to accurately model the phase equilibrium compositions of all binary mixtures except helium–neon with a single binary interaction parameter. For applications where only phase equilibrium compositions are of interest, a cubic equation of state with the interaction parameters provided here is a simple and rather accurate approach. However, their inaccurate representation of pure-component densities and virial coefficients carries over to mixture properties, and the same must be expected for predictions of caloric properties.

There is a clear need for more experimental measurements on mixtures of helium, neon, hydrogen and deuterium at low temperatures. No measurements of caloric properties have been reported, whereas mixture densities have been measured only for the neon–hydrogen and the neon–deuterium mixtures. The experimental coverage of phase equilibrium compositions, however, is decent for most binary mixtures. The industrially important helium–neon mixture is an exception: there are only two sources, which are not only mutually inconsistent, but also inconsistent with the accurately known pure-component saturation pressures of neon. Finally, at least one measurement of a ternary mixture, for example helium–neon–hydrogen, would be valuable to validate the predictive abilities of these force fields beyond two components.

The force fields presented in this work were shown to enable accurate simulations of thermodynamic proper-

This is the accepted version of an article publishet in Journal of Chemical Physics
http://dx.doi.org/10.1063/1.5136079

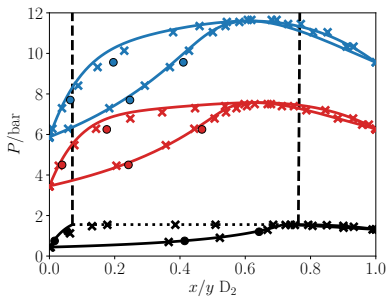

(a) Mie-FH1 Pxy phase diagram.

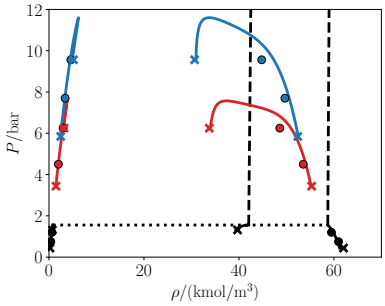

(b) Mie-FH1 $P\rho$ phase diagram.

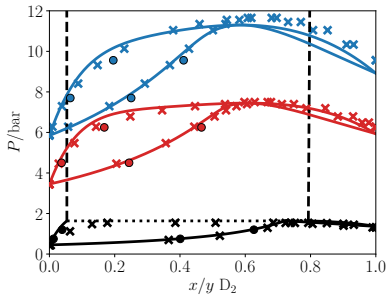

(c) Mie-FH2 Pxy phase diagram.

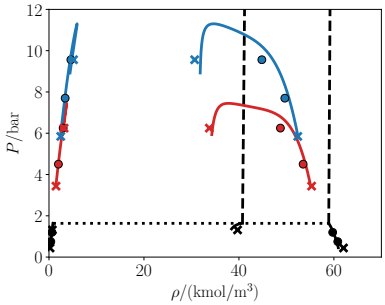

(d) Mie-FH2 $P\rho$ phase diagram.

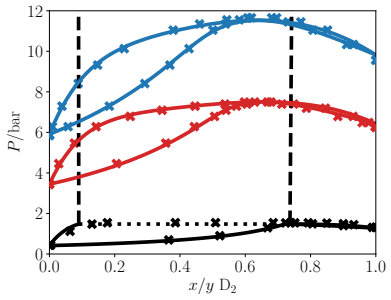

(e) SRK Pxy phase diagram.

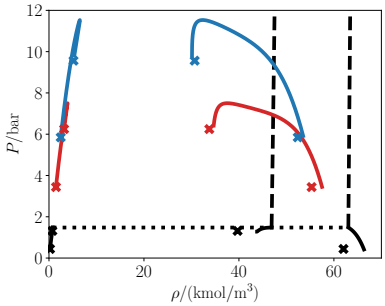

(f) SRK $P\rho$ phase diagram.

FIG. 12. Phase equilibrium diagrams for the deuterium–neon mixture using the Mie-FH1 potential (Figs. 12a and 12b) and Mie-FH2 potential (Figs. 12c and 12d). Crosses are experimental measurements,[60,61] circles are simulation results, and lines are calculations with SAFT-VRQ Mie (Figs. 12a–12d) or SRK (Figs. 12e–12f). The full lines are VLE, the dashed lines are LLE, and the dotted lines indicate VLLE. The crosses in the density plots are the pure-component values computed from reference EoS.[15,17] The temperatures are 24.60 K (black), 31.86 (red) K and 34.47 K (blue).

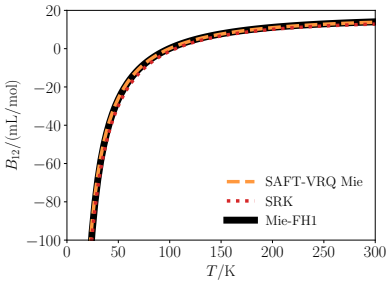

(a) Mie-FH1.

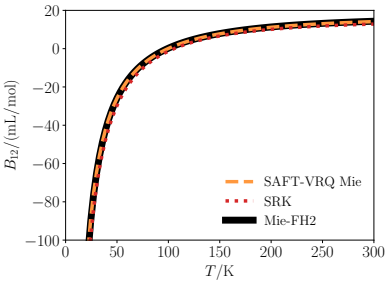

(b) Mie-FH2.

FIG. 13. Cross second virial coefficients for the deuterium–neon mixture using the Mie-FH1 potential (Fig. 13a) and Mie-FH2 potential (Fig. 13b), compared to predictions of SAFT-VRQ Mie and SRK.

This is the accepted version of an article publishet in Journal of Chemical Physics
http://dx.doi.org/10.1063/1.5136079

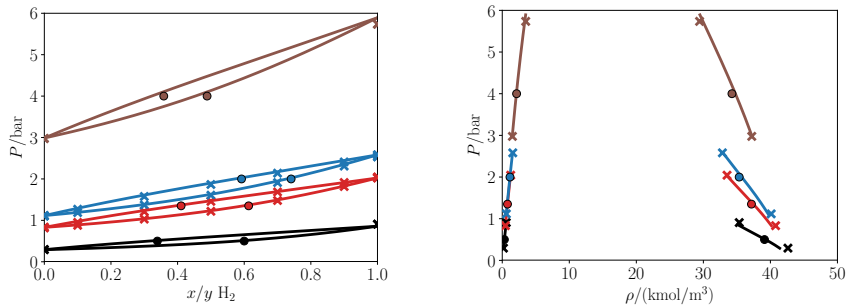

(a) Mie-FH1 Pxy phase diagram. (b) Mie-FH1 $P\rho$ phase diagram.

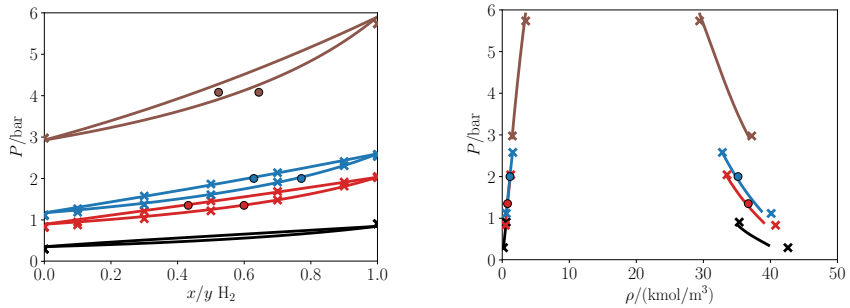

(c) Mie-FH2 Pxy phase diagram. (d) Mie-FH2 $P\rho$ phase diagram.

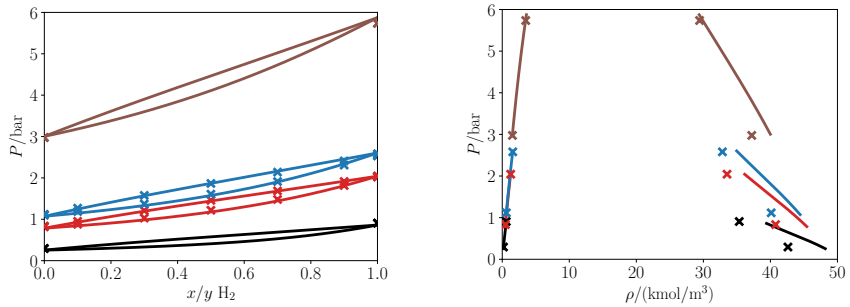

(e) SRK Pxy phase diagram. (f) SRK $P\rho$ phase diagram.

FIG. 14. Phase equilibrium diagrams for the hydrogen–deuterium mixture using the Mie-FH1 potential (Figs. 14a and 14b) and Mie-FH2 potential (Figs. 14c and 14d). Crosses are experimental measurements,[63] circles are simulation results, and lines are calculations with SAFT-VRQ Mie (Figs. 14a–14d) or SRK (Figs. 14e–14f). The crosses in the density plots are the pure-component values computed from reference EoS.[16,17] The temperatures are 20 K (black), 23 K (red), 24 K (blue) and 28 K (brown).

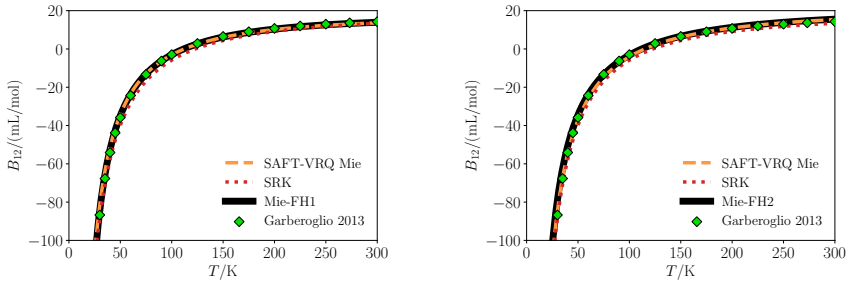

(a) Mie-FH1. (b) Mie-FH2.

FIG. 15. Cross second virial coefficients for the hydrogen–deuterium mixture using the Mie-FH1 potential (Fig. 15a) and Mie-FH2 potential (Fig. 15b), compared to predictions of SAFT-VRQ Mie, SRK and ab initio calculations by Garberoglio et al.[35]

This is the accepted version of an article publishet in Journal of Chemical Physics
http://dx.doi.org/10.1063/1.5136079

ties of mixtures of helium, neon, hydrogen and deuterium at low temperatures. The force fields can also be used to study transport and relaxation properties, for example in the manner as done for He–H_2 and He–D_2 mixtures in Refs. 66 and 67. Considering the high accuracy with which these force fields reproduce the existing experimental measurements, they currently constitute the most accurate, predictive and cost-effective modeling approach for obtaining thermodynamic properties of ultracryogenic fluid mixtures.

SUPPLEMENTARY MATERIAL

See Supplementary Material for (1) single-component virial coefficients; (2) global temperature–pressure binary phase diagrams; (3) tabulated simulation results for binary mixtures.

ACKNOWLEDGMENTS

The authors thank Åsmund Ervik for helpful discussions. Ailo Aasen and Øivind Wilhelmsen are grateful for the support by the ENERSENSE initiative and the PoreLab Center of Excellence. Ailo Aasen, Morten Hammer and Øivind Wilhelmsen have been supported by the HYVA project, which is part of the Strategic Institute Programme of SINTEF Energy Research funded through the Basic Research Funding scheme of the Research Council of Norway. Erich A. Müller was supported by the Engineering and Physical Sciences Research Council (EPSRC) of the UK through grants no. EP/EP016340, EP/J014958 and EP/R013152 to the Molecular Systems Engineering Group.

[1] A. Aasen, M. Hammer, Å. Ervik, E. A. Müller, and Ø. Wilhelmsen, J. Chem. Phys. **151**, 064508 (2019)
[2] T. Lafitte, A. Apostolakou, C. Avendaño, A. Galindo, C. S. Adjiman, E. A. Müller, and G. Jackson, J. Chem. Phys. **139**, 154504 (2013)
[3] U. Cardella, L. Decker, and H. Klein, in *IOP Conference Series: Materials Science and Engineering*, Vol. 171 (2017) p. 012012
[4] Ø. Wilhelmsen, D. Berstad, A. Aasen, P. Nekså, and G. Skaugen, Int. J. Hydrogen Energy **43**, 5033 (2018)
[5] R. Albert, C. Goodzeit, F. Pechar, and A. Prodell, in *Advances in Cryogenic Engineering* (Springer, 1966) pp. 321–327
[6] D. Güsewell, F. Schmeissner, and J. Schmid, Cryogenics **10**, 150 (1970)
[7] S. Satyapal, J. Petrovic, C. Read, G. Thomas, and G. Ordaz, Catal. Today **120**, 246–256 (2007)
[8] R. J. Stochl, J. E. Maloy, P. A. Masters, and R. L. DeWitt, *Gaseous-helium requirements for the discharge of liquid hydrogen from a 3.96-meter (13-ft) diameter spherical tank*, Tech. Rep. (NASA, Cleveland, Ohio, USA, 1970)
[9] G. Soave, Chem. Eng. Sci. **27**, 1197 (1972)
[10] D. Y. Peng and D. B. Robinson, Ind. Eng. Chem. Fund. **15**, 59 (1976)
[11] M.-J. Huron and J. Vidal, Fluid Phase Equilib. **3**, 255 (1979)
[12] O. Jørstad, *Equations of State for Hydrocarbon Mixtures*, Dissertation, Norwegian Institute of Technology (NTH) (1993)
[13] J. Gross and G. Sadowski, Ind. Eng. Chem. Res. **40**, 1244 (2001)
[14] D. O. Ortiz-Vega, *A new wide range equation of state for helium-4*, Ph.D. thesis, Texas A&M University (2013)
[15] R. Katti, R. Jacobsen, R. Stewart, and M. Jahangiri, Adv. Cryog. Eng. **31**, 1189 (1986)
[16] J. W. Leachman, R. T. Jacobsen, S. G. Penoncello, and E. W. Lemmon, J. Phys. Chem. Ref. Data **38**, 721 (2009)
[17] I. A. Richardson, J. W. Leachman, and E. W. Lemmon, J. Phys. Chem. Ref. Data **43**, 013103 (2014)
[18] R. Span, *Multiparameter Equations of State* (Springer-Verlag, Berlin, 2000)
[19] Ø. Wilhelmsen, A. Aasen, G. Skaugen, P. Aursand, A. Austegard, E. Aursand, M. A. Gjennestad, H. Lund, G. Linga, and M. Hammer, Ind. Eng. Chem. Res. **56**, 3503 (2017)
[20] P. J. Leonard, D. Henderson, and J. A. Barker, Trans. Faraday Soc. **66**, 2439 (1970)
[21] Ø. Wilhelmsen, T. T. Trinh, A. Lervik, V. K. Badam, S. Kjelstrup, and D. Bedeaux, Phys. Rev. E **93**, 032801 (2016)
[22] J. A. Barker and D. Henderson, J. Chem. Phys. **47**, 2856 (1967)
[23] J. A. Barker and D. Henderson, J. Chem. Phys. **47**, 4714 (1967)
[24] E. A. Müller and K. E. Gubbins, Ind. Eng. Chem. Res. **40**, 2193 (2001)
[25] P. Paricaud, A. Galindo, and G. Jackson, Fluid Phase Equilib. **194-197**, 87 (2002), proceedings of the Ninth International Conference on Properties and Phase Equilibria for Product and Process Design
[26] E. A. Mueller and G. Jackson, Ann. Rev. Chem. Biomol. Eng. **5**, 405 (2014)
[27] S. A. Febra, A. Aasen, C. S. Adjiman, G. Jackson, and A. Galindo, Mol. Phys., 1(2019)
[28] S. Dufal, T. Lafitte, A. Galindo, G. Jackson, and A. J. Haslam, AIChE J. **61**, 2891 (2015)
[29] J. A. Barker and D. Henderson, Rev. Mod. Phys. **48**, 587 (1976)
[30] A. Gil-Villegas, A. Galindo, P. J. Whiteheat, S. J. Mills, and G. Jackson, J. Comput. Phys. **106**, 4168 (1997)
[31] A. Santos, M. Loópes de Haro, and S. B. Yustec, J. Chem. Phys. **122**, 024514 (2005)
[32] A. Mulero, *Theory and Simulation of Hard-Sphere Fluids and Related Systems* (Springer, Berlin, 2008) ISBN 9783540787662
[33] N. F. Carnahan and K. E. Starling, J. Chem. Phys. **51**, 635 (1969)
[34] D. A. McQuarrie, *Statistical Mechanics* (Harper & Row, New York, 1976)
[35] G. Garberoglio and A. H. Harvey, Int. J. Thermophys. **34**, 385 (2013)
[36] G. Garberoglio, K. Patkowski, and A. H. Harvey, Int. J. Thermophys. **35**, 1435 (2014)
[37] A. Péneloux, E. Rauzy, and R. Fréze, Fluid Phase Equilib. **8**, 7 (1982)
[38] G. M. Kontogeorgis and G. Folas, *Thermodynamic Models for Industrial Applications* (Wiley, 2010)
[39] A. Aasen, M. Hammer, G. Skaugen, J. Jakobsen, and Ø. Wilhelmsen, Fluid Phase Equilib. **442**, 125 (2017)
[40] A. Panagiotopoulos, N. Quirke, M. Stapleton, and D. Tildesley, Mol. Phys. **63**, 527 (1988)
[41] M. Allen and D. Tildesley, *Computer Simulation of Liquids*, 2nd ed. (Oxford University Press, New York, 2017)
[42] D. Frenkel and B. Smit, *Understanding Molecular Simulation: From Algorithms to Applications*, 2nd ed. (Academic Press, New York, 2002)
[43] J. Brewer and G. Vaughn, J. Chem. Phys. **50**, 2960 (1969)
[44] W. Streett, Astrophys. J. **186**, 1107 (1973)
[45] M. Hiza, Fluid Phase Equilib. **6**, 203 (1981)
[46] T. Yamanishi, K. Okuno, Y. Naruse, and E. Sada, J. Phys. Chem. **96**, 2284 (1992)
[47] A. Kidnay, M. Hiza, and R. Miller, Cryogenics **13**, 575 (1973)
[48] P. H. v. Konynenburg and R. L. Scott, Philosophical Transactions of the Royal Society of London Series A **298**, 495 (1980)
[49] M. Cismondi and M. L. Michelsen, J. Supercrit. Fluid. **39**, 287 (2007)
[50] M. Cismondi, M. L. Michelsen, and M. S. Zabaloy, Ind. Eng. Chem. Res. **47**, 9728 (2008)

This is the accepted version of an article publishet in Journal of Chemical Physics
http://dx.doi.org/10.1063/1.5136079

[51]M. Knorn, Cryogenics **7**, 177 (1967)
[52]C. Heck and P. Barrick, in *Adv. Cryog. Eng.* (Springer, 1967) pp. 714–718
[53]M. Hammer, A. Aasen, Å. Ervik, and Ø. Wilhelmsen, J. Chem. Phys.(2020), (submitted)
[54]W. B. Streett and C. H. Jones, J. Chem. Phys. **42**, 3989 (1965)
[55]C. K. Heck and P. Barrick, in *Adv. Cryog. Eng.* (Springer, 1966) pp. 349–355
[56]M. Simon, Phys. Letters **5**, 319 (1963)
[57]W. B. Streett, R. E. Sonntag, and G. J. Van Wylen, J. Chem. Phys. **40**, 1390 (1964)
[58]R. E. Sonntag, G. J. Van Wylen, and R. W. Crain, J. Chem. Phys. **41**, 2399 (1964)
[59]C. M. Sneed, R. E. Sonntag, and G. J. Van Wylen, J. Chem. Phys. **49**, 2410 (1968)
[60]M. Simon, Phys. Letters **2**, 234 (1962)
[61]W. Streett, in *Proc. 2nd Int. Cryog. Eng. Conf.* (Iliffe Science and Technology Publ. Ltd., Guildford, England, 1968) pp. 260–263
[62]H. Hoge and R. Arnold, Journal of Research National Bureau Standards **47**, 63 (1951)
[63]R. Newman and J. LC, Trans. Faraday Soc. **54**, 481 (1958)
[64]A. Treviño, Revista Mexicana de Fisica **4**, 23 (1955)
[65]Y. Le Guennec, S. Lasala, R. Privat, and J.-N. Jaubert, Fluid Phase Equilib. **427**, 513 (2016)
[66]F. R. McCourt, D. Weir, C. Gregory B, and M. Thachuk, Mol. Phys. **103**, 17 (2005)
[67]F. R. W. Mccourt, D. Weir, M. Thachuk, and G. B. Clark, Mol. Phys. **103**, 45 (2005)

This is the accepted version of an article publishet in Journal of Chemical Physics
http://dx.doi.org/10.1063/1.5136079